

Multi-focus Noisy Image Fusion using Low-Rank Representation

Hui Li^a, Xiao-jun Wu^{a,*}

^a*School of Internet of Things Engineering, Jiangnan University, Wuxi 214122, China.*

Abstract

In the process of image acquisition, the noise is inevitable for source image. The multi-focus noisy image fusion is a very challenging task. However, there is no truly adaptive noisy image fusion approaches at present. As we all know, Low-Rank representation(LRR) is robust to noise and outliers. In this paper, we propose a novel fusion method based on LRR for multi-focus noisy image fusion. In the discrete wavelet transform(DWT) framework, the low frequency coefficients are fused by spatial frequency, the high frequency coefficients are fused by LRR coefficients and choose-max strategy. Finally, the fused image is obtained by inverse DWT. Experimental results demonstrate that the proposed algorithm can obtain state-of-the-art performance when the source images contain noise. The Code of our fusion method is available at https://github.com/hli1221/imagefusion_noisy_lrr.

Keywords: multi-focus image fusion, low-rank representation, noisy image fusion

1. Introduction

Multi-focus image fusion is an important technique in image processing field. The main purpose of image fusion is to obtain a single image by fusing complementary information from source images[1].Image fusion methods can be divided

*Corresponding author
Email address: xiaojun_wu_jun@163.com (Xiao-jun Wu)

into two categories: non-representation learning-based methods and representation learning-based methods. In representation learning-based methods, the input images or features are mapped into another domain which makes the problem to be solved easily. And adaptive strategies are utilized to fuse salient features [19][20][21]. Then, fused images will be obtained by these features and input images. In contrast with representation learning-based methods, we called non-representation learning-based methods.

In non-representation learning-based fusion methods, multi-scale transforms are the most commonly fusion methods, such as discrete wavelet transform(DWT)[2], contourlet[3] and shearlet[4][18]. Due to the wavelet transform has not enough detail preservation ability, in reference[5], non-sampled contourlet transform(NSCT) was applied to image fusion.

In addition, the morphology which is also a non-representation learning technique was applied to image fusion. Zhang et al.[6] proposed a fusion method based on morphological gradient. The detail information (like texture and edge) is obtained by different morphological gradient operators. Then the boundary region of focus and defocus, focus region and defocus region are extracted by this information. Finally, the fused image can be obtained by an appropriate fusion strategy.

In representation learning-based fusion methods, the convolutional neural network(CNN)[22], low-rank representation(LRR), and sparse representation(SR) techniques have various applications in image processing.

Liu et al.[7] proposed the CNN-based image fusion methods. A decision map is obtained by the output of CNN which is trained by image patches and different blurred version. Finally, the fused image is obtained by the decision map. However, this method needs lot of images to train the network, even when the images are divided into patches.

For the first time, LRR is applied to image fusion tasks by Li et al.[11]. In their algorithm, K-singular value decomposition (K-SVD) is used to calculate a global dictionary which is utilized to obtained low-rank coefficients of source images. Then, l_1 -norm and choose-max strategy are used to fuse these coef-

ficients. Finally, fused image is reconstructed by global dictionary and fused low-rank coefficients. Due to the dictionary learning is applied to LRR, time efficiency of this methods is very low.

The sparse representation(SR) method[8], [9] is a classical technique in representation learning-based methods. SR-based image fusion has great performance in some image fusion tasks, but it still suffers from many drawbacks: 1) It is difficult to learn a good dictionary in offline manner; 2) The time efficiency of SR-based methods is very low, especially when using online manner to learn dictionary. Due to these drawbacks, Liu et al.[10] proposed a novel image fusion method based on convolutional sparse representation (ConvSR). The CSR-based fusion method obtained better fusion performance.

Besides the above drawbacks, the SR-based image fusion method cannot capture the global structure of image. Furthermore, when the source images contain noise, the image fusion performance obtained by above fusion methods will become worse.

In order to address these problems, we apply LRR to multi-focus image fusion task. As we all know, the LRR is robust to noise and outliers[12]. So the LRR technique is a prefect tool for multi-focus noisy image fusion. In this study, we propose a novel multi-focus image fusion method based on LRR in noisy image fusion task and this method will be introduced in the next section.

The rest of this paper is organized as follows. In Section 2, we introduce the LRR theory briefly. In Section 3, the proposed LRR-based image fusion method will be introduced in detail. The experimental setting and fusion results are provided in Section 4. Section 5 draws the conclusions.

2. Related work

Discrete Wavelet Transform(DWT). In image fusion tasks, DWT[2] is a classical and useful technique for image processing. With DWT operation, input images are decomposed into several coefficient matrices which are low frequency band and high frequency band. The size of coefficient matrices will

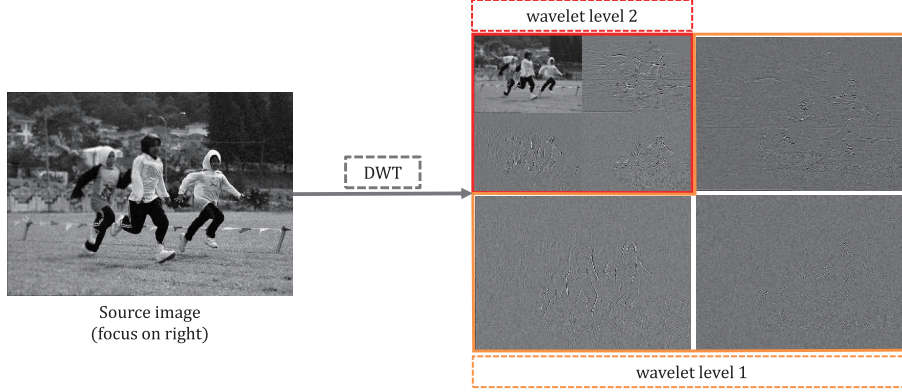


Figure 1: The procedure of DWT operation.

reduce with increase of the level of wavelet decomposition.

In our paper, the procedure of DWT operation is shown in Fig.1.

In Fig.1, the decomposition level of DWT is 2. After DWT operation, seven matrices are obtained. ‘wavelet level 1’ contains three high frequency matrices(upper right: feature of horizontal; bottom left: feature of vertical; bottom right: feature of diagonal). ‘wavelet level 2’ contains one low frequency matrix(upper left) and three high frequency matrices, in which the feature orientations are the same as ‘wavelet level 1’.

Low-rank Representation(LRR). In order to capture the global structure of data, Liu et al.[12] proposed a novel representation method, namely, low-rank representation(LRR).

In reference [12], authors apply self-expression model to avoid training a dictionary and the LRR problem is solved by the following optimization problem,

$$\begin{aligned} \min_{Z, E} \|Z\|_* + \lambda \|E\|_{2,1} \\ s.t., X = XZ + E \end{aligned} \quad (1)$$

where X denotes the observed data matrix, E indicates the noise matrix, $\|\cdot\|_*$ denotes the nuclear norm which is the sum of the singular values of matrix. $\|E\|_{2,1} = \sum_{j=1}^n \sqrt{\sum_{i=1}^n [E]_{ij}^2}$ is called as $l_{2,1}$ -norm, $\lambda > 0$ is the balance coefficient. Eq.1 is solved by the inexact Augmented Lagrange Multiplier (ALM).

Finally, the LRR coefficients matrix Z for X is obtained by Eq.1.

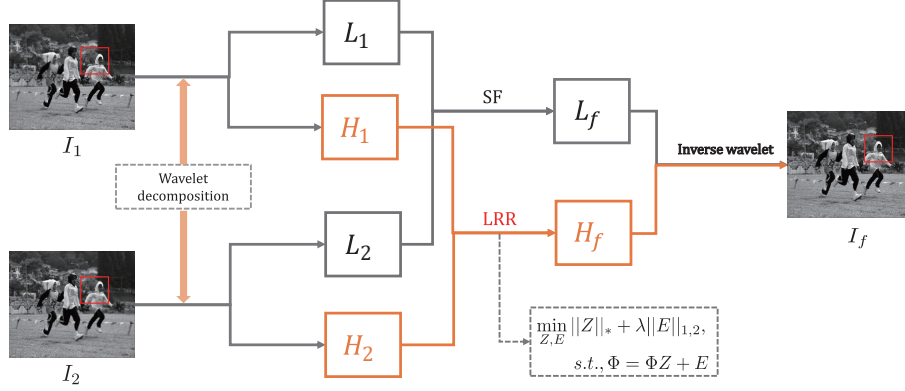


Figure 2: The framework of the proposed method.

3. The Proposed Image Fusion method

In this section, we intend to propose a novel method based on LRR theory in DWT domain. In this paper, the source images (focus on right and left) are denoted as I_1 and I_2 . Note that the fusion strategy is the same when the input images more than 2. And the indices (1, 2) are irrelevant with the focus type. The system diagram of our proposed method is shown in Fig.2.

Firstly, the source images I_1 and I_2 are decomposed by DWT operation. We choose the decomposition level of DWT as 2.

Then, the spatial frequency (SF) and choose-max strategy are used to fuse the low frequency coefficients since the low frequency coefficients reflect the non-detail information of source images. The high frequency coefficients include more detail information of source image, so we choose the LRR to get a low rank matrix and use the nuclear norm and choose-max scheme to fuse the high frequency coefficients. In Fig.2 (LRR), Φ indicates the input high frequency coefficients.

Finally, the fused image is obtained by inverse DWT operation.

3.1. Fusion of low frequency coefficients

The low frequency coefficients contain more contour information and less detail texture information. Thus, the spatial frequency(SF)[7] is used to fuse low frequency coefficients. The SF is calculated by Eq.2 - 4,

$$SF = \sqrt{f_x^2 + f_y^2} \quad (2)$$

$$f_x = \sqrt{\frac{1}{MN} \sum_{i=0}^{M-1} \sum_{j=1}^{N-1} [f(i, j) - f(i, j-1)]^2} \quad (3)$$

$$f_y = \sqrt{\frac{1}{MN} \sum_{i=1}^{M-1} \sum_{j=0}^{N-1} [f(i, j) - f(i-1, j)]^2} \quad (4)$$

where f_x and f_y are spatial frequency of x and y directions, M and N are the row and column numbers of the image.

By sliding window technique, the coefficient matrices are divided into M_l patches. Then the SF value of adjacent coefficient patches are obtained by Eq.2-4. Finally, we use the choose-max scheme to get the fused low frequency coefficients.

Let SF_K^r denote the SF value of each patch, where $K \in \{1, 2\}$ denotes the SF value from which source images, and $r \in \{1, \dots, M_l\}$ denotes r -th patch in source image. Thus, the fused low frequency coefficients L_f is obtained by Eq.5.

$$L_f^r = \begin{cases} L_1^r & SF_1^r > SF_2^r \\ L_2^r & \text{otherwise} \end{cases} \quad (5)$$

3.2. Fusion of high frequency coefficients

Let $H_K^{i,O}$ denote the high frequency coefficients which are obtained by the 2-level DWT, where $O \in \{H, D, V\}$ represents the direction of decomposition and H stand for horizontal, D for diagonal, V for vertical, and $K \in \{1, 2\}$ denotes the index of source images, $i \in \{1, 2\}$ represents the level of DWT operation, each level has 3 high frequency coefficients matrices. Thus, we get 6 high frequency coefficients matrices and one low frequency matrix. The fusion strategy of high frequency coefficients are shown in Fig.3.

By sliding window technique, each high frequency coefficients matrix is divided into M_h patches. The size of window is $n \times n$, $H_{K,j}^{i,O}$ denotes one image

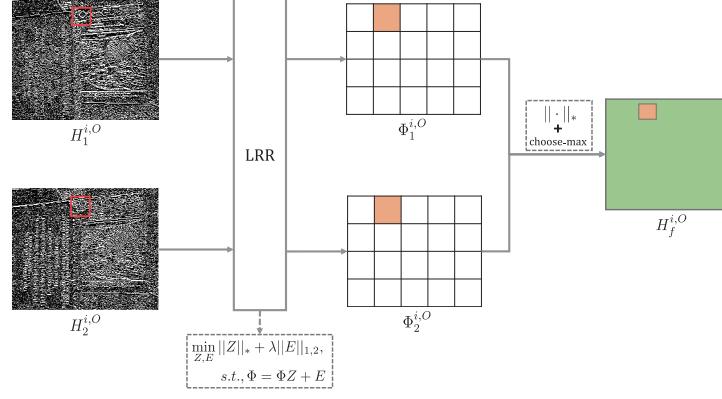


Figure 3: The framework of the fusion of high frequency coefficient.

patch, $j \in \{1, \dots, M_h\}$ denotes j -th patch, $i \in \{1, 2\}$ represents the level of DWT, $O \in \{H, D, V\}$ indicates the direction of decomposition. Then two low-rank matrices $\Phi_{1,j}^{i,O}$ and $\Phi_{2,j}^{i,O}$ are obtained by the LRR theory. The local fused high frequency coefficients matrix $H_{f,j}^{i,O}$ is obtained by comparing the nuclear norm of corresponding low-rank coefficients Z .

Suppose the local high frequency coefficients matrix is denoted by $\Phi_{K,j}^{i,O}$. Applying the self-expression model, and we use $\Phi_{K,j}^{i,O}$ itself as the dictionary. The Eq.6 is used to obtain the low-rank matrix.

$$\begin{aligned} \min_{Z_{K,j}^{i,O}, E} & \|Z_{K,j}^{i,O}\|_* + \lambda \|E\|_{2,1} \\ \text{s.t.} & \Phi_{K,j}^{i,O} = \Phi_{K,j}^{i,O} Z_{K,j}^{i,O} + E \end{aligned} \quad (6)$$

We choose the inexact ALM to solve the problem 6. Then the low-rank coefficients matrix $Z_{K,j}^{i,O}$ and the noise matrix E are obtained. Note that E is noise matrix, so E is ignored in this step. The nuclear norm $\|Z_{K,j}^{i,O}\|_*$ is obtained by computing the sum of the singular values of the matrix $Z_{K,j}^{i,O}$. Finally, the fused high frequency coefficients matrices are calculated by Eq.7,

$$H_{f,j}^{i,O} = \begin{cases} \Phi_{1,j}^{i,O} & \|Z_{1,j}^{i,O}\|_* > \|Z_{2,j}^{i,O}\|_* \\ \Phi_{2,j}^{i,O} & \text{otherwise} \end{cases} \quad (7)$$

where $\Phi_{K,j}^{i,O} = \Phi_{K,j}^{i,O} Z_{K,j}^{i,O}$ denotes the low-rank representation coefficients of $H_{K,j}^{i,O}$.

3.3. Reconstruction of fused image

Having the fused coefficients L_f and H_f , the fused image I_f is reconstructed by inverse DWT.

$$I_f = IDWT(L_f, H_f) \quad (8)$$

In Eq.8, $IDWT(\cdot)$ indicates the inverse DWT operation.

The procedure of our method is described as follows.

1) The source images are decomposed by 2-level DWT. Then the low frequency coefficients L_K and the high frequency coefficients $H_K^{i,O}$ are obtained, where $K \in \{1, 2\}$ (source images), $O \in \{H, D, V\}$ (direction of decomposition), $i \in \{1, 2\}$ (level of DWT).

2) By sliding window technique, the low frequency coefficients are divided into M_l patches and the high frequency coefficients are divided into M_h patches.

3) For low frequency coefficients, we use SF and choose-max scheme to fuse these coefficients.

4) For high frequency coefficients, LRR is used to compute the low-rank matrix Z . Then, $\|Z\|_*$ and choose-max scheme are utilized to get fused high frequency coefficients.

5) Finally, with the fused low frequency coefficients and high frequency coefficients, the fused image is obtained by inverse DWT

4. Experiment

In this section, firstly, we introduce our experimental database. And how to choose the LRR parameter(λ), image patch size and wavelet level in different situations(different noises) are shown in Section 4.2 and 4.3.

Then, we introduce the detail experimental settings and analyze the fused results. Finally, the fusion results are shown in the last section.

The experiments are implemented in MTALAB R2016a on 3.2 GHz Intel(R) Core(TM) CPU with 12 GB RAM.

4.1. Experimental data

In our experiment, we choose ten images from ImageNet in sport(<http://www.image-net.org/index>), as shown in Fig.4. We blur these images to get source images. Gaussian smoothing filter with size 3×3 and $\sigma = 7$ is used to blur these images.



Figure 4: Ten images form ImageNet. In next section, we use image1-10 represent these images.

Furthermore, the noise of Gaussian ($\mu = 0, \sigma = 0.0005, 0.001, 0.005, 0.01$), salt & pepper (the noise density is 0.01 and 0.02) and the noise of Poisson are utilized to process these blurred version images. Then we use these images to determine the parameter(λ) in different situations and compare the results of fusion methods.

The “image1” contains three different noise and focus on different regions are shown in Fig.5.

In order to evaluate the proposed method and other fusion methods, three quality metrics are utilized. These are: Root Mean Square Error(RMSE), Peak Signal to Noise Ratio (PSNR) and Structural Similarity (SSIM). In particular,

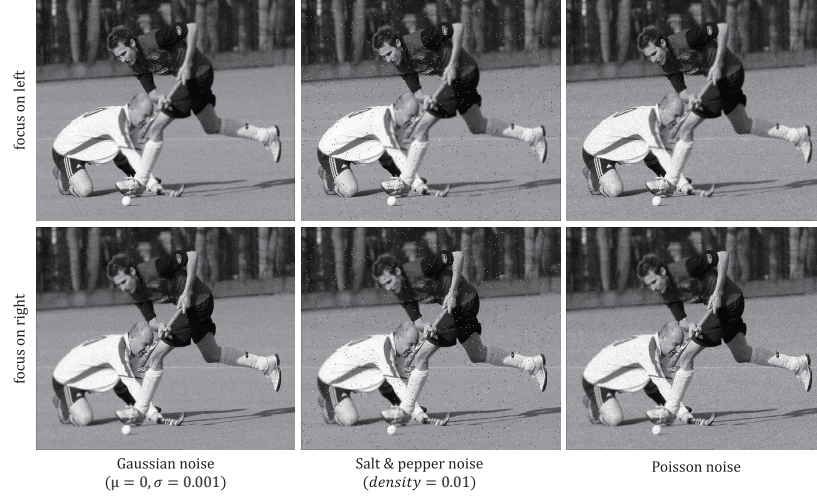


Figure 5: Example for different noise (image1).

RMSE, PSNR and SSIM are based on reference image. The fused image is better when the values of PSNR and SSIM are larger. On the contrary, the fused image is more similar to reference image when the values of RMSE is smaller.

4.2. Effects of parameter

In Eq.6, the parameter $\lambda > 0$ is used to balance the effects of the low rank part(Z) and noise part(E). In this section, we choose image1-5(Fig.4 a-e) and their blurry versions which contain three different types of noise as the source images to determine the parameter λ in our fusion framework.

And in this section, the image patch size and wavelet level are set as 16×16 and 2, respectively. And the settings for patch size and wavelet level are only temporary, we will discuss how to choose the size of image patch and the level of wavelet in next section.

The range of λ is set as $[1, 50]$ for Gaussian noise($\mu = 0, \sigma = 0.0005, 0.001, 0.005, 0.01$) and salt & pepper noise(noise density is 0.01 and 0.02), and the range of λ is set as $[1, 20]$ for Poisson noise. The different situations include Gaussian noise, Salt & pepper noise and Poisson noise. We choose the average SSIM value to

determine the parameter λ which will be used in fusion phase.

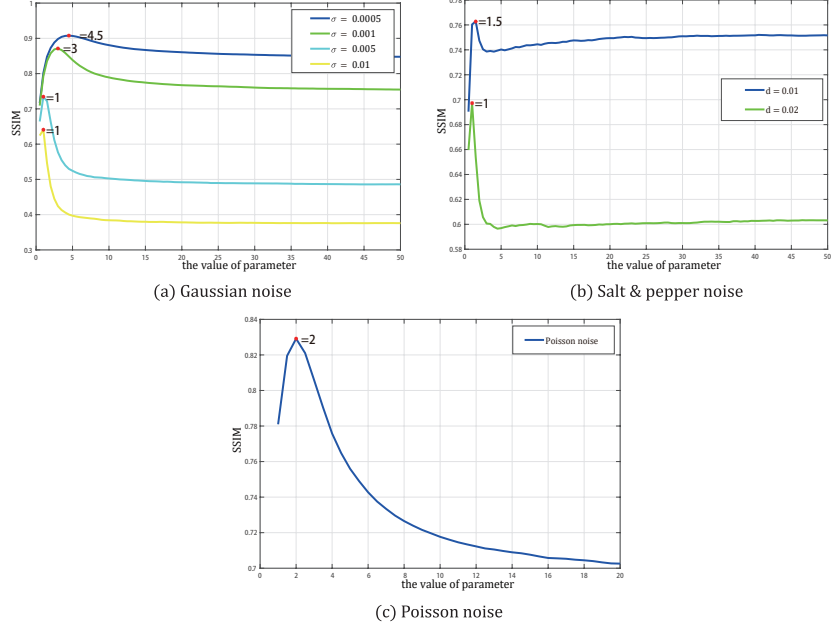


Figure 6: Average SSIM values with different noise. (a) Gaussian noise with different σ ; (b) Salt & pepper noise with different density; (c) Poisson noise.

As shown in Fig.6, when the source images contain Gaussian noise(a), with the increase of *sigma*, the parameter λ will reduce to separate more noise part from input matrix. And SSIM will get maximum value at $\lambda = 4.5, 3, 1, 1$ when *sigma* = 0.0005, 0.001, 0.005, 0.01, respectively.

And the trend is the same for Salt & pepper noise in which the noise density is set as 0.01 and 0.02. SSIM will get maximum value at $\lambda = 1.5, 1$ when $d = 0.01, 0.02$, respectively. When source images contain Poisson noise, λ is set as 2 to get the maximum SSIM value.

Therefore, we choose $\lambda = 4.5, 3, 1, 1$ for containing Gaussian noise in which $\sigma = 0.0005, 0.001, 0.005, 0.01$, respectively. $\lambda = 1.5, 1$ when the source images contain salt & pepper noise($d = 0.01, 0.02$), and $\lambda = 2$ for Poisson noise.

4.3. Patch size and wavelet level

Once the parameter λ is fixed for different noises, we change the image patch size and wavelet level to choose the best patch size and level in our fusion framework. The LRR parameter λ is set as we discussed in Section refpara.

In this section, we calculate the average values of RMSE, PSNR and SSIM for ten pairs of source images. We choose three levels of wavelet, named level 1, level 2, level 3. And four types of images patch size ($4 \times 4, 8 \times 8, 16 \times 16, 32 \times 32$). The average values of RMSE, PSNR and SSIM are shown in Table 1. The best values are denoted in bold and the second-best values are indicated in red.

Table 1: The average values of RMSE, PSNR and SSIM with different patch size and wavelet levels.

Noise	-	Metrics	level 1				level 2				level 3			
			4×4	8×8	16×16	32×32	4×4	8×8	16×16	32×32	4×4	8×8	16×16	32×32
Gaussian noise	$\sigma = 0.0005$	RMSE	0.04913	0.04913	0.04939	0.04979	0.02983	0.02534	0.02327	0.03377	0.12103	0.11986	0.11951	0.12260
		PSNR	26.48348	26.48923	26.44441	26.37138	30.59645	31.98071	32.72188	29.64172	18.47811	18.57138	18.60120	18.35893
		SSIM	0.81914	0.82137	0.81838	0.81049	0.87445	0.90230	0.91120	0.86410	0.81078	0.84021	0.84660	0.80616
	$\sigma = 0.001$	RMSE	0.05033	0.05024	0.05053	0.05111	0.03639	0.03113	0.02839	0.03733	0.12348	0.12149	0.12078	0.12367
		PSNR	26.24008	26.26435	26.21773	26.11500	28.89271	30.21484	30.99987	28.72740	18.28901	18.44223	18.49942	18.27654
		SSIM	0.78905	0.79368	0.79110	0.78133	0.83254	0.86378	0.87428	0.82320	0.76709	0.80377	0.81196	0.76728
	$\sigma = 0.005$	RMSE	0.06024	0.05942	0.05920	0.05959	0.06267	0.05625	0.05059	0.05209	0.13737	0.13283	0.25661	0.13058
		PSNR	24.53899	24.66591	24.70275	24.64929	24.22779	25.13552	26.02700	25.78012	17.30404	17.60930	11.92927	17.76885
		SSIM	0.63780	0.64995	0.65484	0.65078	0.66772	0.70601	0.73387	0.70366	0.58684	0.64162	0.52215	0.64186
	$\sigma = 0.01$	RMSE	0.07059	0.06930	0.06938	0.07161	0.06537	0.05947	0.05714	0.06597	0.13778	0.13354	0.25543	0.13507
		PSNR	23.10186	23.26629	23.25091	22.98052	23.83543	24.62688	24.92995	23.66065	17.27658	17.55954	11.96730	17.46202
		SSIM	0.54179	0.55403	0.55536	0.53552	0.63020	0.66433	0.64582	0.55248	0.58010	0.62457	0.46971	0.51068
Salt & pepper noise	$d = 0.01$	RMSE	0.06027	0.05873	0.05794	0.05799	0.05652	0.05195	0.04882	0.05275	0.13255	0.12944	0.12790	0.12970
		PSNR	24.54166	24.78140	24.91218	24.91224	25.07708	25.77278	26.28470	25.62336	17.62857	17.84646	17.95766	17.82983
		SSIM	0.71254	0.73231	0.74354	0.74463	0.70838	0.73976	0.76127	0.74540	0.63481	0.67707	0.69568	0.68313
	$d = 0.02$	RMSE	0.06814	0.06546	0.06427	0.06465	0.06465	0.05943	0.05606	0.05990	0.13792	0.13386	0.13203	0.13361
		PSNR	23.42172	23.78491	23.95458	23.90851	23.94129	24.63398	25.10640	24.52367	17.26762	17.53855	17.66385	17.55841
		SSIM	0.63032	0.66192	0.67632	0.67273	0.65153	0.68369	0.69728	0.66568	0.57734	0.62144	0.63058	0.60254
Poisson noise	-	RMSE	0.05186	0.05161	0.05181	0.05241	0.04490	0.03874	0.03459	0.04105	0.12726	0.12428	0.12282	0.12501
		SSIM	0.76342	0.76972	0.76891	0.76051	0.78243	0.81914	0.83724	0.79547	0.71025	0.75717	0.77362	0.73820

From Table 1, when the patch size and wavelet level are set as 16×16 and 2, we will get almost the best and the second-best values for different noises.

So in the next experiment, in our method, the wavelet level and image patch size are set as 2 and 16×16 , respectively. And the LRR parameter λ is set as 4.5, 3, 1 and 1 for Gaussian noise ($\mu = 0, \sigma = 0.0005, 0.001, 0.005, 0.01$), 1.5 and 1 for salt & pepper noise ($d = 0.01, 0.02$). $\lambda = 2$ for Poisson noise.

4.4. Fusion results

In this section, ten pairs of images (contain different noise for source images) are used to assess the performance of these methods numerically.

The fusion performance of the proposed method is evaluated against other base line methods, we choose nine state-of-the-art existing methods, including: discrete wavelet transform (DWT)[2], cross bilateral filter fusion method (CBF)[13], discrete cosine harmonic wavelet transform fusion method(DCHWT)[14], multi-scale weighted gradient-based fusion method[15], weighted least square optimization(WLS)[16], convolutional sparse representation(ConvSR)[10], a deep convolutional neural network based fusion method(CNN)[7], multi-layers fusion method(MLVGG)[17] and LRR with dictionary learning based fusion method(DLLRR)[11].

The fused results which are obtained by our method and other nine fusion methods are shown in Fig.7.

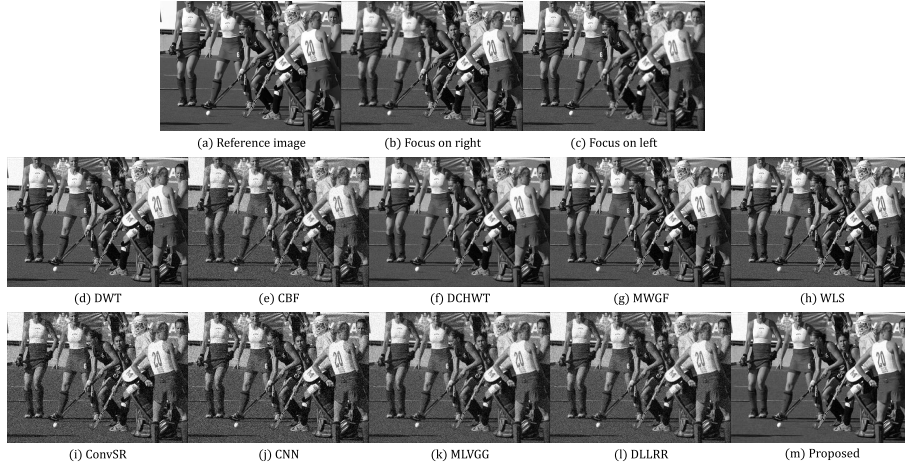


Figure 7: The fused results obtained by fusion methods, and source images contain Gaussian noise($\sigma = 0.001$). (a) Reference image(image 5); (b) Source image(focus on right); (c) Source image(focus on left); (d) DWT; (e) CBF; (f) DCHWT; (g) MWGF; (h) WLS; (i) ConvSR; (j) CNN; (k) MLVGG; (l) DLLRR; (m) Proposed

In Fig.7, source images contain Gaussian noise($\mu = 0, \sigma = 0.001$), this just shows an example for our fused results intuitively.

If fused image is more similar to reference image, then the fusion method

has better fusion performance. As shown in Fig.7, the fused images obtained by CBF, ConvSR, CNN, MLVGG and DLLRR contain some noises, obviously. Compared with DWT, DCHWT, MWGF and WLS, the fused image obtained by our method is more similar to reference image, which means our fusion method can achieve better fusion performance.

The average values of RMSE, PSNR and SSIM for ten fused images obtained by existing methods and our fusion algorithm are shown in Table 2. And in our experiment, source images still contain three different types of noise. The best values are indicated in bold and the second-best values are denoted in red

Table 2: The average values of RMSE, PSNR and SSIM for ten fused images which obtained by fusion methods.

Noise	–	Metrics	DWT	CBF	DCHWT	MWGF	WLS	ConvSR	CNN	MLVGG	DLLRR	Ours
Gaussian noise	$\sigma = 0.0005$	RMSE	0.03113	0.02537	0.02351	0.02307	0.03167	0.02226	0.02292	0.02862	0.03497	0.02327
		PSNR	30.14548	31.93089	32.58992	32.74183	30.00285	33.06375	32.79989	31.02855	29.14272	32.72188
		SSIM	0.81004	0.89162	0.88547	0.87179	0.81724	0.89293	0.87405	0.88661	0.77964	0.91120
	$\sigma = 0.001$	RMSE	0.04131	0.03041	0.02981	0.03188	0.04139	0.02999	0.03139	0.03268	0.03502	0.02839
		PSNR	27.68133	30.35320	30.52164	29.92970	27.66704	30.46610	30.06572	29.81845	29.12999	30.99987
		SSIM	0.71738	0.83131	0.82113	0.79239	0.72592	0.81877	0.79725	0.83239	0.77930	0.87428
	$\sigma = 0.005$	RMSE	0.08671	0.05597	0.05848	0.06917	0.08632	0.06474	0.06737	0.05463	0.06891	0.05059
		PSNR	21.23926	25.04502	24.66211	23.20208	21.27921	23.77792	23.43194	25.27746	23.23508	26.02700
		SSIM	0.45425	0.59962	0.58219	0.53231	0.46152	0.55600	0.54500	0.61366	0.52955	0.73387
	$\sigma = 0.01$	RMSE	0.12028	0.07610	0.08002	0.09679	0.12007	0.09050	0.09342	0.07262	0.09549	0.05714
		PSNR	18.39774	22.37396	21.93746	20.28483	18.41309	20.86844	20.59205	22.79417	20.40204	24.92995
		SSIM	0.34680	0.48149	0.46482	0.41124	0.35154	0.43372	0.42838	0.49764	0.41158	0.64582
Salt & pepper noise	$d = 0.01$	RMSE	0.07673	0.07303	0.06396	0.06227	0.07765	0.06004	0.05557	0.04743	0.06898	0.04882
		PSNR	22.30494	22.73372	23.88697	24.12445	22.20101	24.43670	25.10832	26.52406	23.22975	26.28470
		SSIM	0.68092	0.69094	0.70344	0.76767	0.68251	0.76205	0.80460	0.77917	0.71655	0.76127
	$d = 0.02$	RMSE	0.10665	0.09720	0.08391	0.08450	0.10836	0.08299	0.07782	0.06248	0.09274	0.05606
		PSNR	19.44543	20.25157	21.52925	21.47467	19.30612	21.62228	22.18351	24.11548	20.66027	25.10640
		SSIM	0.51530	0.53728	0.56410	0.63543	0.51534	0.62258	0.66816	0.65694	0.57302	0.69728
Poisson noise	–	RMSE	0.05077	0.03531	0.03576	0.04018	0.05072	0.03745	0.03919	0.03694	0.04211	0.03459
		PSNR	25.90846	29.06021	28.94820	27.94211	25.92070	28.55098	28.15376	28.72500	27.53885	29.28811
		SSIM	0.67047	0.78986	0.77762	0.74238	0.67943	0.77032	0.75138	0.79366	0.73287	0.83724

From Table 2, when source images contain less noise, such as Gaussian noise with $\sigma = 0.0005$ and Salt & pepper noise with $d = 0.01$, we don't have an obvious advantage. However, with the increase of noises, our method achieves almost best values in RMSE, PSNR and SSIM. This phenomenon indicates that our fusion algorithm can obtain better fusion performance when source images contain noise.

5. Conclusions

In this paper, a novel noisy image fusion method based on low-rank representation has been proposed. In the DWT framework, the low frequency coefficients are fused by spatial frequency and choose-max scheme. And the high frequency coefficients are fused by low-rank representation and choose-max scheme. The experimental results show that the proposed method is more reasonable and more similar to original image. From the fused images and the values of RMSE, PSNR and SSIM, our method has better fusion performance compared with other methods when source images contain noise.

References

- [1] S. Li, X. Kang, L. Fang, J. Hu, and H. Yin, Pixel-level image fusion: A survey of the state of the art, *Inf. Fusion*, vol. 33, pp. 100-112, 2017.
- [2] A. Ben Hamza, Y. He, H. Krim, and A. Willsky, A Multiscale Approach to Pixel-level Image Fusion, *Integr. Comput. Aided. Eng.*, vol. 12, pp. 135-146, 2005.
- [3] S. Yang, M. Wang, L. Jiao, R. Wu, and Z. Wang, Image fusion based on a new contourlet packet, *Inf. Fusion*, vol. 11, no. 2, pp. 78-84, 2010.
- [4] L. Wang, B. Li, and L. F. Tian, EGGDD: An explicit dependency model for multi-modal medical image fusion in shift-invariant shearlet transform domain, *Inf. Fusion*, vol. 19, no. 1, pp. 29-37, 2014.
- [5] Q. Zhang and B. long Guo, Multifocus image fusion using the nonsubsampling contourlet transform, *Signal Processing*, 2009.
- [6] Y. Zhang, X. Bai, and T. Wang, Boundary finding based multi-focus image fusion through multi-scale morphological focus-measure, *Inf. Fusion*, 2017.
- [7] Y. Liu, X. Chen, H. Peng, and Z. Wang, Multi-focus image fusion with a deep convolutional neural network, *Inf. Fusion*, vol. 36, pp. 191-207, 2017.

- [8] M. Nejati, S. Samavi, and S. Shirani, Multi-focus image fusion using dictionary-based sparse representation, *Inf. Fusion*, vol. 25, pp. 72-84, 2015.
- [9] H. Yin, Y. Li, Y. Chai, Z. Liu, and Z. Zhu, A novel sparse-representation-based multi-focus image fusion approach, *Neurocomputing*, vol. 216, pp. 216-229, 2016.
- [10] Y. Liu, X. Chen, R. K. Ward, and J. Wang, Image Fusion with Convolutional Sparse Representation, *IEEE Signal Process. Lett.*, vol. 23, no. 12, pp. 1882-1886, 2016.
- [11] H. Li and X.-J. Wu, Multi-focus Image Fusion using dictionary learning and Low-Rank Representation, in *Image and Graphics. ICIG 2017. Lecture Notes in Computer Science*, vol 10666. Springer, Cham., 2017, pp. 675-686.
- [12] G. Liu, Z. Lin, and Y. Yu, Robust Subspace Segmentation by Low-Rank Representation, in *Proceedings of the 27th International Conference on Machine Learning*, 2010, pp. 663-670.
- [13] B. K. Shreyamsha Kumar, Image fusion based on pixel significance using cross bilateral filter, *Signal, Image Video Process.*, 2015.
- [14] B. K. Shreyamsha Kumar, Multifocus and multispectral image fusion based on pixel significance using discrete cosine harmonic wavelet transform, *Signal, Image Video Process.*, vol. 7, no. 6, pp. 1125-1143, 2013.
- [15] Z. Zhou, S. Li, and B. Wang, Multi-scale weighted gradient-based fusion for multi-focus images, *Inf. Fusion*, vol. 20, no. 1, pp. 60-72, 2014.
- [16] J. Ma, Z. Zhou, B. Wang, and H. Zong, Infrared and visible image fusion based on visual saliency map and weighted least square optimization, *Infrared Phys. Technol.*, vol. 82, pp. 8-17, 2017.
- [17] H. Li, X.-J. Wu, and J. Kittler, Infrared and Visible Image Fusion using a Deep Learning Framework, in *arXiv preprint arXiv:1804.06992*, 2018.
- [18] Luo X, Zhang Z, Wu X. A novel algorithm of remote sensing image fusion based on shift-invariant Shearlet transform and regional selection[J]. *AEU-*

International Journal of Electronics and Communications, 2016, 70(2): 186-197.

- [19] Zheng Y J, Yang J Y, Yang J, et al. Nearest neighbour line nonparametric discriminant analysis for feature extraction[J]. Electronics Letters, 2006, 42(12): 679-680.
- [20] Sun J, Fang W, Wu X J, et al. Quantum-behaved particle swarm optimization: principles and applications[J]. 2011.
- [21] Wang M, Wang S T, Wu X J. Initial results on fuzzy morphological associative memories[J]. Acta Electronica Sinica, 2003, 31(5): 690-693.
- [22] Li H, Wu X J. DenseFuse: A fusion approach to infrared and visible images[J]. IEEE Transactions on Image Processing, 2018, 28(5): 2614-2623.